Temperature-Dependent Screening of the Edge State around Antidots in the Quantum Hall Regime

Masanori Kato,* Akira Endo, Shingo Katsumoto, and Yasuhiro Iye
Institute for Solid State Physics, University of Tokyo, 5-1-5 Kashiwanoha, Kashiwa, Chiba 277-8581, Japan
(Received 12 October 2008; published 23 February 2009)

The Aharonov-Bohm effect in a small array of antidots with a large aspect ratio is investigated in the quantum Hall regime. The evolution with temperature of the Aharonov-Bohm oscillations in the magnetic field versus gate voltage (B-V_g) plane reveals the temperature dependence of the screening. The self-consistently screened potential of the compressible band surrounding an antidot is observed to gain a progressively steeper slope with increasing temperature.

DOI: 10.1103/PhysRevLett.102.086802 PACS numbers: 73.23.−b, 73.43.−f

The integer quantum Hall (QH) effect, observed in a two-dimensional electron gas (2DEG) subjected to a strong perpendicular magnetic field [1], is generally explained within a noninteracting electron picture. In such a picture, the edge state along the system boundary is simply envisaged as the crossing point of the Landau level (LL), which rises in energy as the boundary is approached, with the Fermi level (E_F). The width of the edge states is then determined by the spatial extension of the relevant single-particle wave function, which is given by the magnetic length $\ell = (\hbar/eB)^{1/2}$. When the screening effect of a 2DEG is taken into consideration, the LLs take a more complicated profile in the vicinity of E_F. The energy dispersion of the edge states becomes stepwise, consisting of compressible and incompressible regions at zero temperature [2]. Theoretical calculations extended to finite temperatures [3,4] predict progressive smearing of the stepwise profile with increasing temperature. Thus the temperature dependence of the edge potential profile reflects the self-consistent screening of a 2DEG at finite temperatures. Experimentally, the temperature-induced change of the edge state was invoked by Machida *et al.* [5] in their interpretation of the interedge-channel transport. In order to attain a more quantitative account of the evolution of the edge states with temperature, the present work addresses this issue via study of the Aharonov-Bohm (AB) effect in an antidot system.

A quantum antidot, i.e., a submicron potential hill for 2D electrons, constitutes an artificial "boundary" and provides a useful system for the study of the QH edge states. Under a strong perpendicular magnetic field, electrons form bound states around the antidot. The magnetotransport of antidot systems in the QH regime ubiquitously exhibits AB oscillations (ABOs) [6–12], which arise from the coupling of the localized orbits to the current-carrying extended states. Part of the magnetocounductance features, e.g., the oscillation period, can be understood within a single-particle (SP) picture. However, many experiments [6–8,11,12] and theories [13,14] point to the crucial role played by the electron-electron interaction. A full understanding of the antidot systems therefore requires detailed knowledge of the structure of edge states which inevitably involves the self-consistent screening effect. Conversely, detailed experiments should furnish relevant information on the QH edge states.

In a preceding paper [15], we have shown that the evolution of the ABOs as a function of magnetic field and carrier density reveals the strong modification of the potential profile around an antidot by the screening effects. Here we focus on the temperature dependence of the ABOs in the magnetic field-density plane. We show that the slope of the screened potential around an antidot becomes steeper with increasing temperature. This can be attributed to the temperature dependence of the screening effect as predicted by the existing theoretical calculations [3,4].

Antidot array samples were fabricated from a GaAs/AlGaAs single heterojunction wafer (density $n = 4.0 \times 10^{11}$ cm^{-2} and mobility $\mu = 98$ m^2/V s). The sample used in this study was a 5.3 μm wide Hall bar containing 5×5 antidots in a square lattice pattern [shown in the inset in Fig. 1(a)] used in the previous work [15,16]. The lattice period was $a = 1$ μm, and the antidot radius was $r = 350$ nm. The effective radius r^* of the antidot was larger than the lithographical radius r typically by $\sim$100 nm, so that the channels between two neighboring antidots were $\sim$100 nm wide at their narrowest point. This sort of antidot array system can be viewed as a network of narrow conducting channels. The Ohmic contacts to the Hall bar were made with AuGe/Ni electrode pads. A Au-Ti Schottky front gate enabled us to tune the Fermi energy of the system. The resistance measurements were made by a standard low-frequency (13 Hz) lock-in technique with low excitation current (typically 1 nA) at different temperatures ranging from 30 to 800 mK.

Figure 1(a) shows the magnetoresistivity ρ_{xx} of the sample at $V_g = 0$ mV around the LL filling factor $\nu = 6$ ($B \simeq 1.8$ T) for different temperatures. The trace contains an oscillatory component $\Delta\rho_{xx}$ in the QH transition region as shown in Fig. 1(b). The period of the oscillation is $\Delta B \simeq 5.7$ mT corresponding to the AB period expected for the

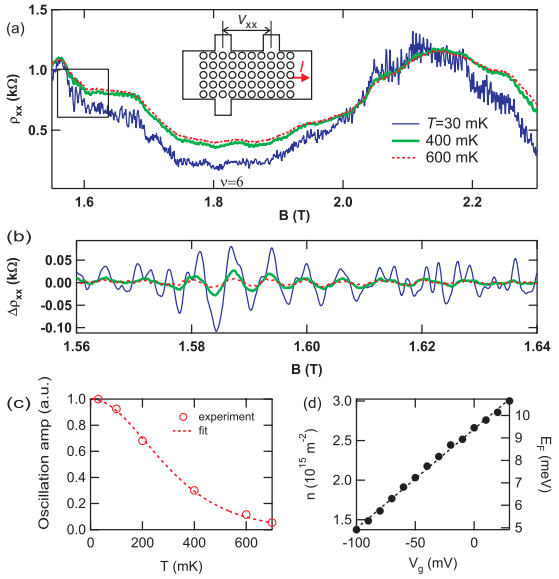

FIG. 1 (color online). (a) ρ_{xx} at $V_g = 0$ mV around $\nu = 6$ for different temperatures. The inset is the schematic geometry of a sample with antidots. (b) The oscillatory component of the trace in the square area in (a) obtained by subtraction of the smooth background. (c) Temperature dependence of the amplitude of the periodic oscillations around $B = 1.6$ T. Open circles represent the experimental data. The dashed line is the fit to the Dingle function $aT/\sinh(aT)$ $(a = 2\pi^2 k_B/\Delta E,\ \Delta E = 0.22$ meV). (d) The dependence of the density on the gate voltage V_g in the antidot sample obtained from the magnetic-field positions of the center of the Hall plateaus (left axis). The corresponding Fermi energy $E_F = \pi\hbar^2 n/m^*$ is indicated in the right axis, where $m^* = 0.067 m_e$ is the effective mass of electron in GaAs. The dependence is linear in the range of V_g studied, with the conversion factor $\Delta E_F/\Delta V_g = 0.046$ eV/V.

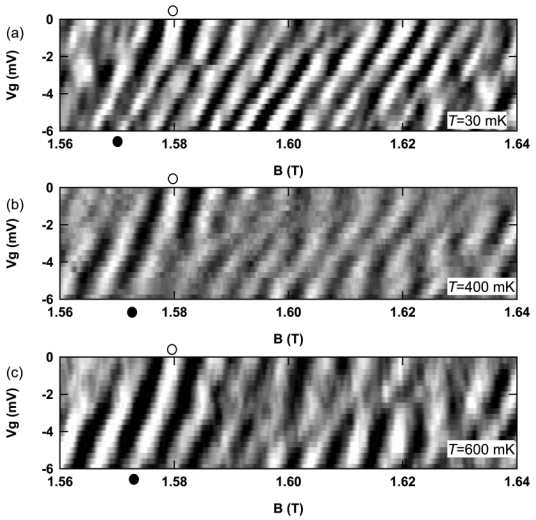

FIG. 2. (a)–(c) Gray-scale plots of $\Delta\rho_{xx}$ obtained by magnetic-field sweeps with various values of V_g. White regions represent higher resistance. Open and solid circles in each figure show the magnetic-field position of a peak at $V_g = 0$ and -6 mV, respectively.

effective antidot area $S = \pi r^{*2}$, with $r^* = 480$ nm. Figure 1(c) shows the decrease of the oscillation amplitude with temperature following the Dingle function, in accordance with our previous observation [17].

Figure 2 shows the evolution of the ABOs in Fig. 1(b) with the gate bias. The light and dark regions represent local peaks and dips of $\Delta\rho_{xx}$, respectively. With increasing temperature, the trajectories of the ABOs in the B-V_g plane becomes steeper; i.e., the slope $\Delta V_g/\Delta B$ of the stripes becomes larger. For example, the peak marked by an open circle at $V_g = 0$ mV stays at the same magnetic-field position $B = 1.58$ T for different temperatures, while the corresponding peak marked by a solid circle at $V_g = -6$ mV is seen to shift to higher magnetic field with increasing temperature. As discussed in our previous paper [15], the value of $\Delta V_g/\Delta B$ reflects the screened potential profile around the antidot at E_F. Let us derive the relevant relation from the Bohr-Sommerfeld quantization condition $\pi r_m^2 B = mh/e$ which determines the period of the ABOs. Here the integer m specifies the mth single-particle state encircling the antidot, and r_m is its radius. The ratio $\Delta V_g/\Delta B$ is given by

$$\frac{\Delta V_g}{\Delta B} = -\frac{r_m}{2B}\left(\frac{\Delta r_m}{\Delta V_g}\right)^{-1} = -\frac{r_m}{2B}\left(\frac{dE}{dr}\right)_{r_m}\left(\frac{\Delta E_F}{\Delta V_g}\right)^{-1}, \quad (1)$$

where $\Delta r_m/\Delta V_g$ denotes the change by the gate bias of the radius r_m at E_F enclosing m magnetic flux quanta. Equation (1) allows us to translate the measured slope $\Delta V_g/\Delta B$ into $|dE/dr|_{r_m}$ at E_F by using the value $\Delta E_F/\Delta V_g = 0.046$ eV/V estimated from Fig. 1(d). Thus the temperature dependence of $\Delta V_g/\Delta B$ reveals the evolution of the potential profile around an antidot with the temperature. Figure 3(a) presents the $\Delta V_g/\Delta B$ for different temperatures at $V_g = 0$ mV. As can be seen in Fig. 2, the slope slightly fluctuates from line to line, disturbed by fluctuations in the background resistance unrelated to the ABOs; the disturbance is more pronounced for higher temperatures where the amplitudes of the ABOs are smaller. To circumvent this disturbance, we plot in Fig. 3(a) the average of the slopes included in the magnetic-field range ± 0.1 T (roughly corresponding to the size of the symbols) of the point plotted in the figure; the range contains typically 25 lines. The value of $\Delta V_g/\Delta B$ is observed to increase with temperature, with the increment more noticeable for lower magnetic fields and almost absent for $B \geq 4$ T. Qualitatively the same behavior is observed at other gate biases.

Figure 3(b) shows the temperature dependence of the potential slope $|dE/dr|_{r^*}$ at E_F obtained from the values of $\Delta V_g/\Delta B$ in Fig. 3(a) with $r_m (= r^*)$ calculated from the period of the ABOs. In all cases, the potential slope $|dE/dr|_{r^*}$ increases with increasing temperature.

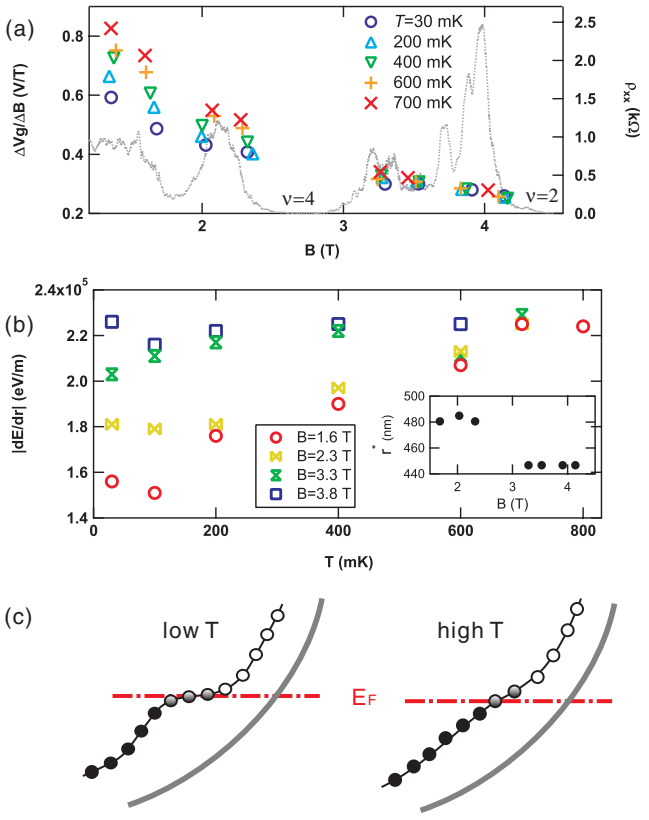

FIG. 3 (color online). (a) The slopes of AB oscillations $\Delta V_g/\Delta B$ at $V_g = 0$ mV for different temperatures. Each symbol is obtained after sufficient averaging over the field range ~0.2 T. The dotted gray line indicates ρ_{xx} as a guide for the eye. (b) The temperature dependence of the potential slope around an antidot for different magnetic fields obtained from the data in (a) and $r_m(= r^*)$ at each magnetic field using Eq. (1). The inset is the effective antidot radius r^* deduced from the period of the ABOs at each magnetic field. (c) Schematic representations of the potential near E_F around an antidot with the screening effect at low and high temperatures. The circles represent the SP states. The filled, half-filled, and open circles correspond to the occupied, partially occupied, and unoccupied states, respectively. The solid gray lines indicate the bare antidot potentials.

However, the effect of temperature is stronger at lower magnetic fields (higher fillings).

Let us take, as an example, the field range around $B \simeq 1.6$ T. Here the value of $|dE/dr|_{r^*}$ changes by ~40% from 1.6×10^5 eV/m at 30 mK to 2.2×10^5 eV/m at 800 mK. These values can be compared with a different line of estimation. The radial separation Δr_m between two adjacent SP states, as estimated from $\Delta r_m \simeq h/2\pi e r_m B$, is 0.9 nm at $B = 1.6$ T. The energy separation ΔE between the SP states, on the other hand, has been estimated from the temperature dependence of the oscillation amplitudes in Fig. 1(c) as 0.22 meV. Combination of these values gives $|dE/dr|_{r^*} \simeq 2 \times 10^5$ eV/m, roughly in agreement with the above values.

The change of $|dE/dr|_{r^*}$ with temperature is attributed to the temperature-dependent screening of the electrostatic potential for the edge states around the antidot as exaggeratedly depicted in Fig. 3(c). The potential profile at the edge of the antidot is greatly modified from the bare potential by the strong screening effect [2]. Theoretical calculations [2,3] suggest that the effective potential in the compressible region becomes nearly flat at low enough temperatures. With increasing temperature, the screening effect diminishes so that the gradient of the self-consistent potential gradually increases towards the bare value. The screening is more effective for a higher density of states and hence for higher magnetic fields. This explains why the slope $|dE/dr|_{r^*}$ is more robust against the temperature at higher magnetic fields. In fact, the theoretical calculation [3] indicates that substantial deviation from the low-temperature limit occurs typically at $k_B T/\hbar\omega_c \geq 0.01$, where $\hbar\omega_c$ is the LL spacing. This requires $T \geq 800$ mK for $B \sim 4$ T, the temperature at which the ABO is no longer visible.

The behavior of $|dE/dr|_{r^*}$ discussed thus far can be, at least qualitatively, explained by the Thomas-Fermi theory by Lier and Gerhardts [3], which considers infinitely long one-dimensional edges of the infinite 2DEG (half-)plane. We now discuss a few aspects that defy a simple explanation within the framework of this theory. First, the observed $|dE/dr|_{r^*}$ remains nonzero at $T \to 0$; i.e., the screened potential in the compressible region is *not completely flat*. The situation is consistent with the single antidot experiment by Karakurt *et al.* [9], who argued that the perfectly compressible regions are not formed around an antidot. This is also in qualitative agreement with the calculations of the edge states in quantum wires [18,19]. Suzuki and Ando [18] demonstrated in a self-consistent Hartree approximation that the complete flattening of the compressible stripes does not appear in a narrow wire with width 100–200 nm. As mentioned before, our sample can be regarded as a network of the wire with the width ~100 nm. Ihnatsenka and Zozoulenko [19] also showed by the density functional theory (DFT) that the formation of the compressible stripes can be suppressed in the narrow-width wires.

Second, the low-temperature ($T = 30$ mK) value of $|dE/dr|_{r^*}$ in Fig. 3(b) tends to be larger at higher fields. The origin of this behavior is not clear at the moment but may be related to the radius of the edge state around an antidot. A numerical calculation using the DFT [14] showed that the compressible band of the edge states formed around an antidot tends to be narrower for a smaller antidot. The inset in Fig. 3(b) shows the radii of the edge states around an antidot with a sudden drop in the vicinity of the $\nu = 4$ ($B \simeq 2.7$ T); with the increase of the magnetic field, the LL that constitutes the outermost edge states around the antidot changes from the second LL to the lowest LL at $\nu = 4$ accompanied by the reduction

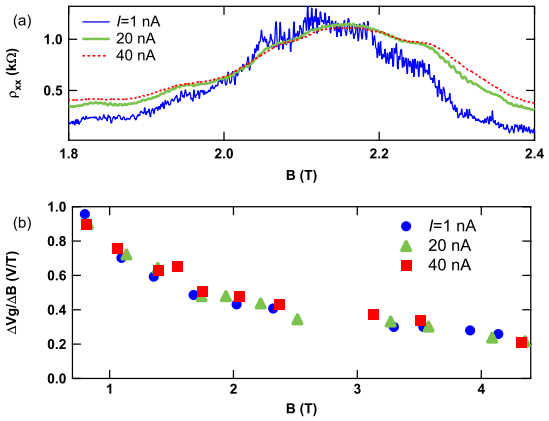

FIG. 4 (color online). (a) ρ_{xx} traces for $V_g = 0$ mV in the filling factor range between $\nu = 4$ and 6 measured with three excitation currents at $T = 30$ mK. (b) The magnetic-field dependence of $\Delta V_g/\Delta B$ for different currents.

of r^*. The larger value of $|dE/dr|_{r^*}$ at higher magnetic fields may, therefore, be ascribable to the smaller antidot radius r^*.

Finally, we compare the above result of the finite temperature effect with the effect of *electron heating* due to applied currents. Figure 4(a) shows ρ_{xx} at $T = 30$ mK for different excitation currents. As the current is increased, the amplitude of the ABO diminishes. This is similar in appearance to the case of raised temperature shown in Fig. 1(a). The values of $\Delta V_g/\Delta B$ in Fig. 4(b), however, do not change with the bias current, implying that the effective potential around the antidot is not affected by electron heating. The effective electron temperature can be estimated from the comparison of the amplitude of Shubnikov–de Haas oscillations or that of the ABOs for each current with those at different lattice temperatures. The estimated values of the electron temperature are $T_e \sim$ 400 and 800 mK at $I = 20$ and 40 nA, respectively.

As discussed in earlier publications [16,20], the ABO is attributed to the oscillatory fine structure of the density of states derived from the localized states around the antidot, detected by the conductive extended states at E_F in the QH transition regions. The applied high current raises the electron temperature, i.e., smears out the energy distribution function, of the extended states, leading to the decrease of the ABO amplitudes. The insensitivity of the potential profile around the antidot to the bias current, on the other hand, suggests that the high current is unable to affect the electron temperature, and hence the screening, of the localized states around the antidot owing to the weakness of the coupling between the current-carrying extended states and the localized edge states around the antidot.

In summary, we have investigated the temperature dependence of the potential profile around an antidot in the integer QH transition regions by the slope of the ABOs in the B-V_g plane. The potential gradient of the edge states is much flatter than the bare potential due to the screening effect. However, the gradient remains finite even in the low-temperature limit, possibly due to the narrow width of the conducting channel. The gradient becomes larger with increasing temperature as a result of the reduction of screening.

This work was supported by the Grant-in-Aid for Scientific Research from the Ministry of Education, Culture, Sports, Science and Technology (MEXT) Japan and was also partly supported by Special Coordination Funds for Promoting Science and Technology.

*masanori@issp.u-tokyo.ac.jp

[1] R. E. Prange and S. M. Girvin, *The Quantum Hall Effect* (Springer, New York, 1990), 2nd ed.
[2] D. B. Chklovskii, B. I. Shklovskii, and L. I. Glazman, Phys. Rev. B **46**, 4026 (1992); D. B. Chklovskii, K. A. Matveev, and B. I. Shklovskii, Phys. Rev. B **47**, 12 605 (1993).
[3] K. Lier and R. R. Gerhardts, Phys. Rev. B **50**, 7757 (1994).
[4] J. H. Oh and R. R. Gerhardts, Phys. Rev. B **56**, 13 519 (1997).
[5] T. Machida, H. Hirai, S. Komiyama, T. Osada, and Y. Shiraki, Phys. Rev. B **54**, R14 261 (1996).
[6] C. J. B. Ford, P. J. Simpson, I. Zailer, D. R. Mace, M. Yosefin, M. Pepper, D. A. Ritchie, J. E. F. Frost, M. P. Grimshaw, and G. A. C. Jones, Phys. Rev. B **49**, 17 456 (1994).
[7] M. Kataoka, C. J. B. Ford, G. Faini, D. Mailly, M. Y. Simmons, and D. A. Ritchie, Phys. Rev. B **62**, R4817 (2000).
[8] M. Kataoka, C. J. B. Ford, M. Y. Simmons, and D. A. Ritchie, Phys. Rev. Lett. **89**, 226803 (2002).
[9] I. Karakurt, V. J. Goldman, J. Liu, and A. Zaslavsky, Phys. Rev. Lett. **87**, 146801 (2001).
[10] F. E. Camino, W. Zhou, and V. J. Goldman, Phys. Rev. B **72**, 155313 (2005).
[11] V. J. Goldman, J. Liu, and A. Zaslavsky, Phys. Rev. B **77**, 115328 (2008).
[12] M. Kato, A. Endo, S. Katsumoto, and Y. Iye, Physica (Amsterdam) **40E**, 1517 (2008).
[13] H.-S. Sim, M. Kataoka, and C. J. B. Ford, Phys. Rep. **456**, 127 (2008).
[14] S. Ihnatsenka and I. V. Zozoulenko, Phys. Rev. B **74**, 201303(R) (2006).
[15] M. Kato, A. Endo, S. Katsumoto, and Y. Iye, J. Phys. Soc. Jpn. **77**, 093715 (2008).
[16] M. Kato, A. Endo, S. Katsumoto, and Y. Iye, Phys. Rev. B **77**, 155318 (2008).
[17] M. Kato, H. Tanaka, A. Endo, S. Katsumoto, and Y. Iye, Physica (Amsterdam) **34E**, 534 (2006).
[18] T. Suzuki and T. Ando, J. Phys. Soc. Jpn. **62**, 2986 (1993); Physica (Amsterdam) **227B**, 46 (1996).
[19] S. Ihnatsenka and I. V. Zozoulenko, Phys. Rev. B **73**, 155314 (2006).
[20] Y. Iye, M. Ueki, A. Endo, and S. Katsumoto, J. Phys. Soc. Jpn. **73**, 3370 (2004).